

*Supporting Information*

*for*

Boosting CO<sub>2</sub> Reduction Catalyzed by Tetragonal Metal Chalcogenides: A DFT  
Study

Fei Yang<sup>a</sup>, Xu Huang<sup>a</sup>, Chengfang Yang<sup>a</sup>, Chao Su<sup>a</sup>, Bei-Bei Xiao<sup>a\*</sup>,

<sup>a</sup>*School of Energy and Power Engineering, Jiangsu University of Science and Technology, 212003, Zhenjiang,  
Jiangsu, China*

---

\* Corresponding author.

Dr. Xiao, B. B. E-mail: xiaobb11@mails.jlu.edu.cn, xbb420@just.edu.cn; Phone: 86-137-7535-8009;

## Computational Method

Spin-unrestricted were performed during all calculations within the DMol<sup>3</sup> code under the framework of DFT.<sup>1, 2</sup> With the Perdew-Burke-Ernzerhof (PBE) functional, the generalized gradient approximation (GGA) was adopted to treat the exchange-correlation interaction effect.<sup>3</sup> The Grimme correction (DFT-D) and DFT Semi-core Pseudo Potentials (DSPP) method was utilized in this study to accurately describe dispersion force and treat core electrons.<sup>4</sup> A thermal smearing of 0.005 Ha (1 Ha = 27.2114 eV) to the orbital occupation was applied to achieve accurate electronic convergence. Double numerical plus polarization (DNP) was used to describe atomic orbitals.<sup>2</sup> The global cutoff quality was employed as fine for high precision. The convergence tolerances of energy, maximum force, and displacement were found to be  $1.0 \times 10^{-5}$  Ha, 0.002 Ha/Å, and 0.005 Å respectively during the geometry structural optimization. All the systems were relaxed without any constraints. Moreover, we used a conductor-like screening model (COSMO) to simulate the aqueous environment, where the dielectric constant of H<sub>2</sub>O was 78.54.<sup>5, 6</sup> A  $2 \times 2 \times 1$  supercell containing 8 TM and 8 S atoms was applied with at least 20 Å vacuum space in the z-direction which was enough to prevent spurious interactions between the tetragonal monolayer and periodic images.

The binding energies ( $E_b$ ) were calculated to examine the stability of the designed catalysts by:

$$E_b = E_{\text{catalyst}} - E_{\text{substrate}} - E_{\text{TM}} \quad (1)$$

where  $E_{\text{catalyst}}$ ,  $E_{\text{substrate}}$ , and  $E_{\text{TM}}$ , are the total energies of the catalyst, the substrate, and the adsorbed metal atoms.

To further reveal the stability of the designed catalysts, the formation energies ( $E_f$ ) are calculated by:

$$E_f = E_{\text{catalyst}} - E_{\text{substrate}} - E_{\text{TM, bulk}} \quad (2)$$

where  $E_{\text{catalyst}}$ ,  $E_{\text{substrate}}$ , and  $E_{\text{TM, bulk}}$ , are the total energies of the catalyst, the substrate, and the bulk energies of adsorbed metal atoms.

The Gibbs free energy difference ( $\Delta G$ ) of the elementary steps was calculated based on the computational hydrogen electrode (CHE) model proposed by Nørskov et al.,<sup>7</sup> where the chemical potential of the ( $\text{H}^+ + e^-$ ) system in solution is substituted by half the chemical potential of one  $\text{H}_2$  molecule.<sup>8-10</sup> Thus, the Gibbs free energy change is calculated by:

$$\Delta G = \Delta E + \Delta ZPE - T\Delta S + \Delta G_U + \Delta G_{\text{pH}} \quad (3)$$

where  $\Delta E_{\text{ZPE}}$  represents the zero-point energy difference obtained based on the reaction using DFT calculations of the vibrational frequencies and standard tables for gas phase molecules and  $T$  is set as 298.15 K herein.  $ZPE$  and  $S$  can be calculated from the vibrational frequencies according to standard methods. The substrates are fully constrained during the frequency calculation according to the suggestion of Wilcox et al.<sup>11</sup>  $\Delta G_U = -eU$  expressed as the free energy contribution from the variation in electrode potential, and the pH correction of the free energy is expressed as  $\Delta G_{\text{pH}} = -k_B T \ln 10 \times \text{pH}$ , where  $k_B$  is the Boltzmann constant and pH is zero in this case. The limiting potential ( $U_L$ ) is defined as required the energy between the elementary hydrogenations and spontaneous reaction, which is calculated by  $U_L = -\Delta G_{\text{max}}/e$ , where  $\Delta G_{\text{max}}$  is the maximum change in free energy along varied elementary steps. The overpotential is calculated by  $\eta = U_{\text{eq}} - U_L$ , wherein  $U_{\text{eq}}$  are 0.17 V for the conversion from  $\text{CO}_2$  to  $\text{CH}_4$ .<sup>12</sup>

## Stability

$E_f$  of Co-FeS, Fe-CoS and Co-CoS are 1.79, 1.52 and 1.48 eV, respectively. There is a clustering possibility of TM adsorption<sup>13, 14</sup>. However, we want to mention that when  $E_b$  that larger than  $-1.5$  eV would provide enough kinetical fixation ability for TM adsorption.<sup>15</sup> Herein,  $E_b$  values are  $-2.95$ ,  $-3.78$  and  $-3.25$  eV for Co-FeS, Fe-CoS and Co-CoS, respectively, which indicates the mentioned candidates are stable kinetically. Furthermore, to provide other evidences to support our ideas, we have listed the formation energies  $E_f$  as well as the binding energies  $E_b$  of TM decorated MoS<sub>2</sub> for direct comparison, which have been well synthesized and adopted in catalysis field. Herein,  $E_f$  are 2.61, 2.47, 1.89 and 1.97 eV and the  $E_b$  values are evaluated to be  $-2.68$ ,  $-2.26$ ,  $-3.23$  and  $-1.85$  eV for Fe-MoS<sub>2</sub>, Co-MoS<sub>2</sub>, Ni-MoS<sub>2</sub> and Cu-MoS<sub>2</sub>, respectively. All the data of our designed systems and TM decorated MoS<sub>2</sub> are in the same range that less than  $-1.5$  eV.<sup>15</sup> As we known, Fe-MoS<sub>2</sub>,<sup>16</sup> Co-MoS<sub>2</sub>,<sup>17</sup> Ni-MoS<sub>2</sub><sup>18</sup> and Cu-MoS<sub>2</sub><sup>19</sup> have been synthesized and were confirmed to be stable. Hence, it is reasonable to infer that the materials we designed are stable.

## **$2e^-$ reduction**

HCOOH is thermodynamically possible when CO<sub>2</sub> reduction catalyzed by Ni-FeS, Cu-FeS, and Ni-CoS due to the easy desorption of HCOOH as demonstrated in Fig. 3b. Herein, Fig. S14a presents the corresponding free energy profiles of CO<sub>2</sub> reduction via  $2e^-$  protonation.  $\Delta G_i$  stands for the free energy change of the  $i^{\text{th}}$  protonation step. Taken Cu-FeS as an illustration, the CO<sub>2</sub> molecule firstly adsorbs on the Cu atom with  $\Delta G_{*CO_2}$  of  $-0.21$  eV, indicating a spontaneous process. In the first protonation process, the H atom firstly attached to C atoms in  $*CO_2$  and the  $*HCO_2$  is formed with the  $\Delta G_1$  of  $0.12$  eV. Subsequently, the  $*HCOOH$  intermediate is generated with  $\Delta G_2$  of  $-0.30$  eV. This means that both steps are thermodynamically favored. However, the HCOOH desorption needs a  $0.76$  eV extra energy. Thus, the HCOOH production catalyzed by Cu-FeS would be suffered from the recovery of active site for continuous working. The similar situations are found for Ni-FeS and Ni-CoS wherein the energy inputs of the protonation steps are extremely low, as indicated by  $\Delta G_{\text{max}}$  of  $0.01$  and  $0.10$  eV, however, the desorption processes are endothermic with  $\Delta G_{\text{des}}(\text{HCOOH})$  of  $0.68$  and  $0.52$  eV, respectively. Note that the room temperature  $T$  of  $300$  K would provide an extra energy of  $0.75$  eV as previous reported,<sup>20</sup> which is expected to be a thermodynamically driving force for HCOOH desorption. Therefore, it is reasonably expected that HCOOH is formed via  $2e^-$  reduction when CO<sub>2</sub> catalyzed by Ni-FeS, Cu-FeS and Ni-CoS, being competitive compared with the previous literatures.<sup>21, 22</sup>

## 8e<sup>-</sup> reduction

Firstly, the CO<sub>2</sub> molecule adsorbed on Co-FeS with  $\Delta G_{*CO_2}$  of -0.01 eV, a step of physical adsorption. The first-protonation step is  $*CO_2 \rightarrow *HCO_2$  with  $\Delta G_1$  of -0.12 eV not the  $*CO_2 \rightarrow *COOH$  with  $\Delta G$  of 0.14 eV.  $\Delta G_2$  of  $*HCO_2 \rightarrow *HCOOH$  and  $\Delta G_3$  of  $*HCOOH \rightarrow *CHO$  are -0.20 eV and 0.06 eV, respectively. The fourth-hydrogenation step of  $*CHO \rightarrow *HCHO$  is identified as the potential-determining step (PDS) due to its maximum  $\Delta G_4$  of 0.41 eV, that is,  $\Delta G_{max}$  of 0.41 eV. The  $*H_3CO$  formation accompanied by  $*H_3CO$  adsorption via O-Co bond, with  $\Delta G_5$  of -0.22 eV. It is worth mentioning that, for Co-FeS and Fe-CoS, the free energies of HCHO desorption  $\Delta G_{des}(HCHO)$  are 0.58 eV and 0.45 eV, respectively, wherein HCHO desorption is thermodynamically preferred. That is, the  $*HCHO$  desorption is occurred. Furthermore,  $\Delta G_{des}(HCHO)$  values are larger than the fifth-protonation step ( $*HCHO \rightarrow *H_3CO$ ) with the  $\Delta G_5$  values are -0.22 and -0.59 eV. Hence, the  $*HCHO$  formation will not affect the entire CRR process to produce CH<sub>4</sub>. Similarly,  $*CH_3OH$  formation is achieved with  $\Delta G_6$  of -0.54 eV. The detachment of the hydroxyl group (-OH) from  $*CH_3OH$  to produce H<sub>2</sub>O is slightly endothermic and the corresponding  $\Delta G_7$  is 0.19 eV. Finally,  $\Delta G_8$  of the  $*CH_4$  formation is -0.42 eV. The CH<sub>4</sub> desorption is a spontaneous process accompanied by  $\Delta G_{des}(CH_4)$  of -0.18 eV. In a word, the optimal reaction pathway when CO<sub>2</sub> catalyzed by Co-FeS is summarized as  $*CO_2(g) \rightarrow *HCO_2 \rightarrow *HCOOH \rightarrow *CHO \rightarrow *HCHO \rightarrow *H_3CO \rightarrow *CH_3OH \rightarrow *CH_3 \rightarrow *CH_4$ . According to the free energy profiles shown in Fig. S12, the same reaction pathway is identified for Fe-CoS wherein the corresponding  $\Delta G_i$  are -0.15, -0.13, 0.77, -0.07, -0.59, -0.14, 0.03 and -0.61 eV, respectively. That is, the PDS of Fe-CoS is the third protonation step of  $*HCOOH \rightarrow *CHO$  with  $\Delta G_{max}$  of 0.77 eV. However, a different reaction pathway is found when CO<sub>2</sub> catalyzed by

Co-CoS. The first-protonation step is  $*\text{CO}_2 \rightarrow *\text{COOH}$  with  $\Delta G_1$  of  $-0.03$  eV not the  $*\text{CO}_2 \rightarrow *\text{HCO}_2$  with  $\Delta G$  of  $0.04$  eV. According to the free energy profiles shown in Fig. S13, the favorable pathway is  $*\text{CO}_2(\text{g}) \rightarrow *\text{COOH} \rightarrow *\text{CO} \rightarrow *\text{CHO} \rightarrow *\text{HCOH} \rightarrow *\text{CH}_2\text{OH} \rightarrow *\text{CH}_3\text{OH} \rightarrow *\text{CH}_3 \rightarrow *\text{CH}_4$  with the corresponding  $\Delta G_i$  of  $-0.03$ ,  $-0.66$ ,  $0.91$ ,  $0.18$ ,  $-0.22$ ,  $-0.64$ ,  $0.00$  and  $-0.39$  eV, respectively. Therefore, the third protonation step of  $*\text{CO} \rightarrow *\text{CHO}$  is identified as the PDS step with  $\Delta G_{\text{max}}$  of  $0.91$  eV.

## Figure Captions

**Fig. S1.** (a) Binding energies  $E_b$  with TM adsorption at site-II. (b) Binding energies  $E_b$  with TM adsorption at site-III. (c) Mulliken charges of TM decoration atom.

**Fig. S2.** (a) PDOS between Co adsorption and its substrate. (b) PDOS between Fe adsorption and its substrate. (c) PDOS between Ni adsorption and its substrate. (d) PDOS between Cu adsorption and its substrate.

**Fig. S3.** (a) Charge density difference (CDD) between Co adsorption and its substrate. (b) Charge density difference (CDD) between Fe adsorption and its substrate. (c) Charge density difference (CDD) between Ni adsorption and its substrate. (d) Charge density difference (CDD) between Cu adsorption and its substrate.

**Fig. S4.** (a) Optimized structures of CO<sub>2</sub> adsorption on Fe decoration. (b) Optimized structures of CO<sub>2</sub> adsorption on Co decoration. (c) Optimized structures of CO<sub>2</sub> adsorption on Ni decoration. (d) Optimized structures of CO<sub>2</sub> adsorption on Cu decoration.

**Fig. S5.** Charge density difference (CDD) and the electron transfer for Co-FeS, Ni-FeS, Cu-FeS, Fe-CoS, Co-CoS and Ni-CoS.

**Fig. S6.** TDOS for free state CO<sub>2</sub> and adsorbed CO<sub>2</sub>.

**Fig. S7.** The comparison between  $\Delta G_{*CO_2}$  and  $\Delta G_{*H}$ .

**Fig. S8.** Gibbs free energy diagrams of the CO<sub>2</sub> reduction to CH<sub>4</sub> for Fe-FeS, Fe-CoS, Fe-FeSe and Fe-CoSe.

**Fig. S9.** Gibbs free energy diagrams of the CO<sub>2</sub> reduction to CH<sub>4</sub> for Co-FeS, Co-CoS, Co-FeSe and Co-CoSe.

**Fig. S10.** Gibbs free energy diagrams of the CO<sub>2</sub> reduction to CH<sub>4</sub> for Ni-FeS, Ni-CoS, Ni-FeSe and

Ni-CoSe.

**Fig. S11.** Gibbs free energy diagrams of the CO<sub>2</sub> reduction to CH<sub>4</sub> for Cu-FeS, Cu-CoS, Cu-FeSe and Cu-CoSe.

**Fig. S12.** Gibbs free energy diagrams of the CO<sub>2</sub> reduction to CH<sub>4</sub> for Fe-CoS along the preferred reaction pathway.

**Fig. S13.** Gibbs free energy diagrams of the CO<sub>2</sub> reduction to CH<sub>4</sub> for Co-CoS along the preferred reaction pathway.

**Fig. S14.** (a) Gibbs free energy diagrams of the CO<sub>2</sub> reduction catalyzed by Ni-FeS, Cu-FeS, and Ni-CoS. (b) Overpotential comparison of our work and the reported literatures<sup>22-26</sup>.

**Fig. S15.** (a) The fitting of the limiting potential  $U_L$  as a function of  $\Delta G_3$ . (b) The fitting of the limiting potential  $U_L$  as a function of  $\Delta G_3 - \Delta G_4$ .

### Table Captions

**Table S1.** Binding energies  $E_b$ , formation energies  $E_f$ , TM Mulliken charges  $Q_{TM}$ , CO<sub>2</sub> adsorption free energies  $\Delta G^*_{CO_2}$ , CO<sub>2</sub> Mulliken charges  $Q_{CO_2}$ , length  $l_{C=O}$  of C=O bond, bond angle  $\theta_{O=C=O}$  of O=C=O, hydrogen adsorption free energies  $\Delta G^*_{H}$  ( $E_b$ ,  $E_f$ ,  $\Delta G^*_{CO_2}$  and  $\Delta G_H$  in eV,  $l_{C=O}$  in Å,  $\theta_{O=C=O}$  in °,  $Q$  and  $Q_{CO_2}$  in  $e$ ).

**Table S2.** Total Gibbs free energies  $G$  of corresponding intermediate species along CO<sub>2</sub> conversion into CH<sub>4</sub> for Fe decoration.

**Table S3.** Total Gibbs free energies  $G$  of corresponding intermediate species along CO<sub>2</sub> conversion into CH<sub>4</sub> for Co decoration.

**Table S4.** Total Gibbs free energies  $G$  of corresponding intermediate species along CO<sub>2</sub> conversion

into CH<sub>4</sub> for Ni decoration.

**Table S5.** Total Gibbs free energies  $G$  of corresponding intermediate species along CO<sub>2</sub> conversion

into CH<sub>4</sub> for Cu decoration.

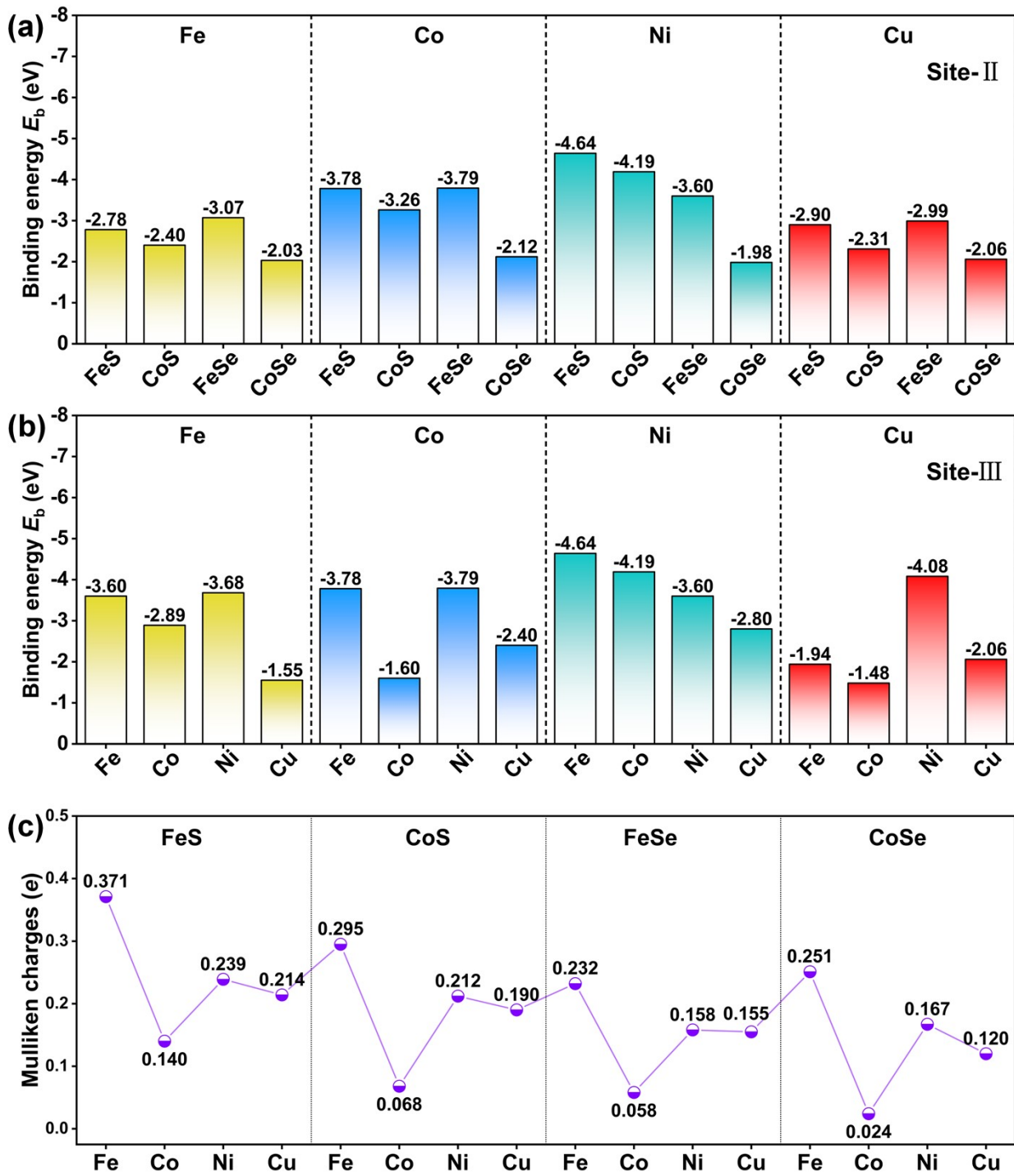


**Fig. S1.** (a) Binding energies  $E_b$  with TM adsorption at site-II. (b) Binding energies  $E_b$  with TM adsorption at site-III. (c) Mulliken charges of TM decoration atom.

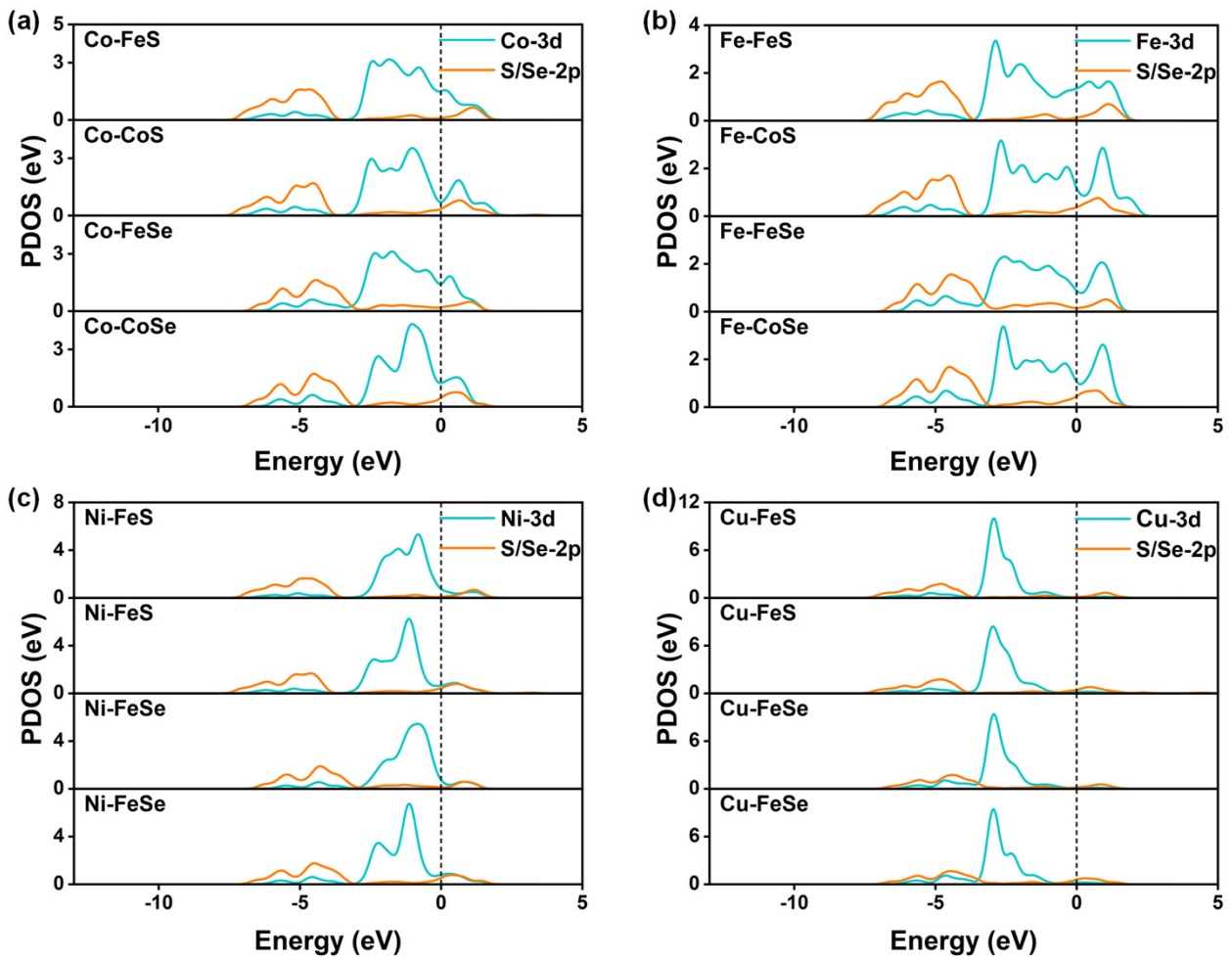


**Fig. S2.** (a) PDOS between Co adsorption and its substrate. (b) PDOS between Fe adsorption and its substrate. (c) PDOS between Ni adsorption and its substrate. (d) PDOS between Cu adsorption and its substrate.

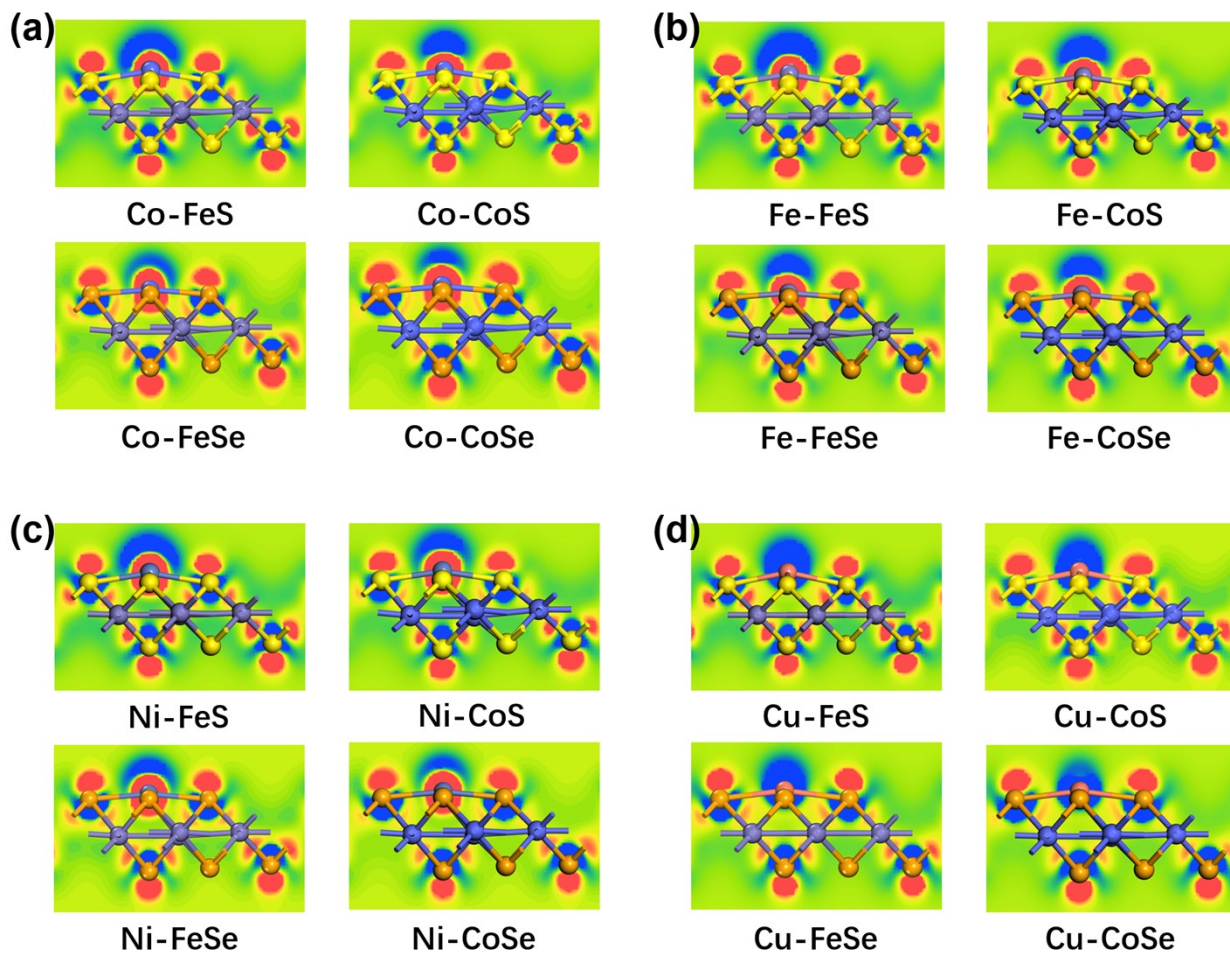


**Fig. S3.** (a) Charge density difference (CDD) between Co adsorption and its substrate. (b) Charge density difference (CDD) between Fe adsorption and its substrate. (c) Charge density difference (CDD) between Ni adsorption and its substrate. (d) Charge density difference (CDD) between Cu adsorption and its substrate.

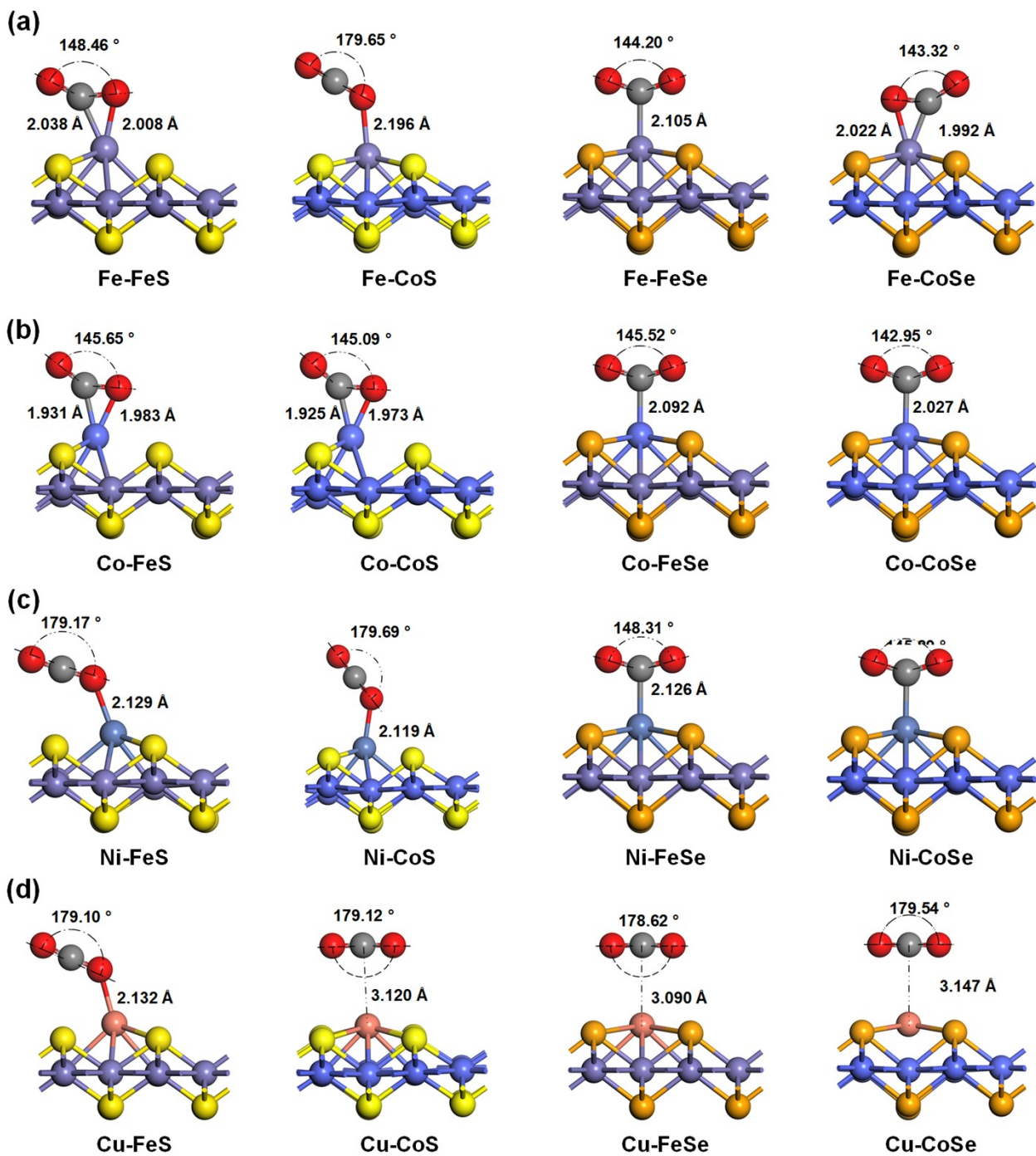


**Fig. S4.** (a) Optimized structures of CO<sub>2</sub> adsorption on Fe decoration. (b) Optimized structures of CO<sub>2</sub> adsorption on Co decoration. (c) Optimized structures of CO<sub>2</sub> adsorption on Ni decoration. (d) Optimized structures of CO<sub>2</sub> adsorption on Cu decoration.

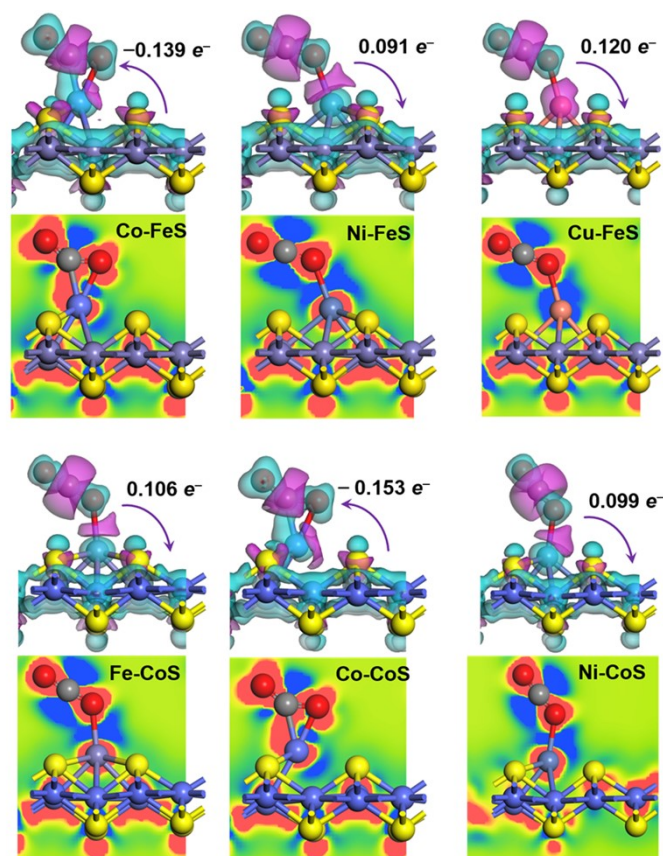


**Fig. S5.** Charge density difference (CDD) and the electron transfer for Co-FeS, Ni-FeS, Cu-FeS, Fe-CoS, Co-CoS and Ni-CoS.

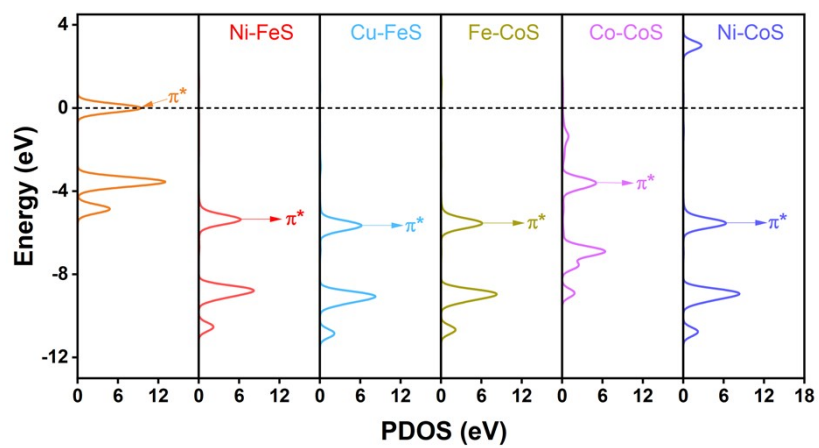


**Fig. S6.** TDOS for free state CO<sub>2</sub> and adsorbed CO<sub>2</sub>.

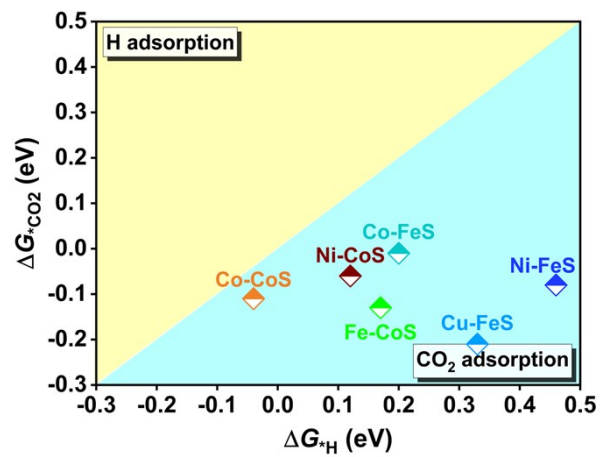
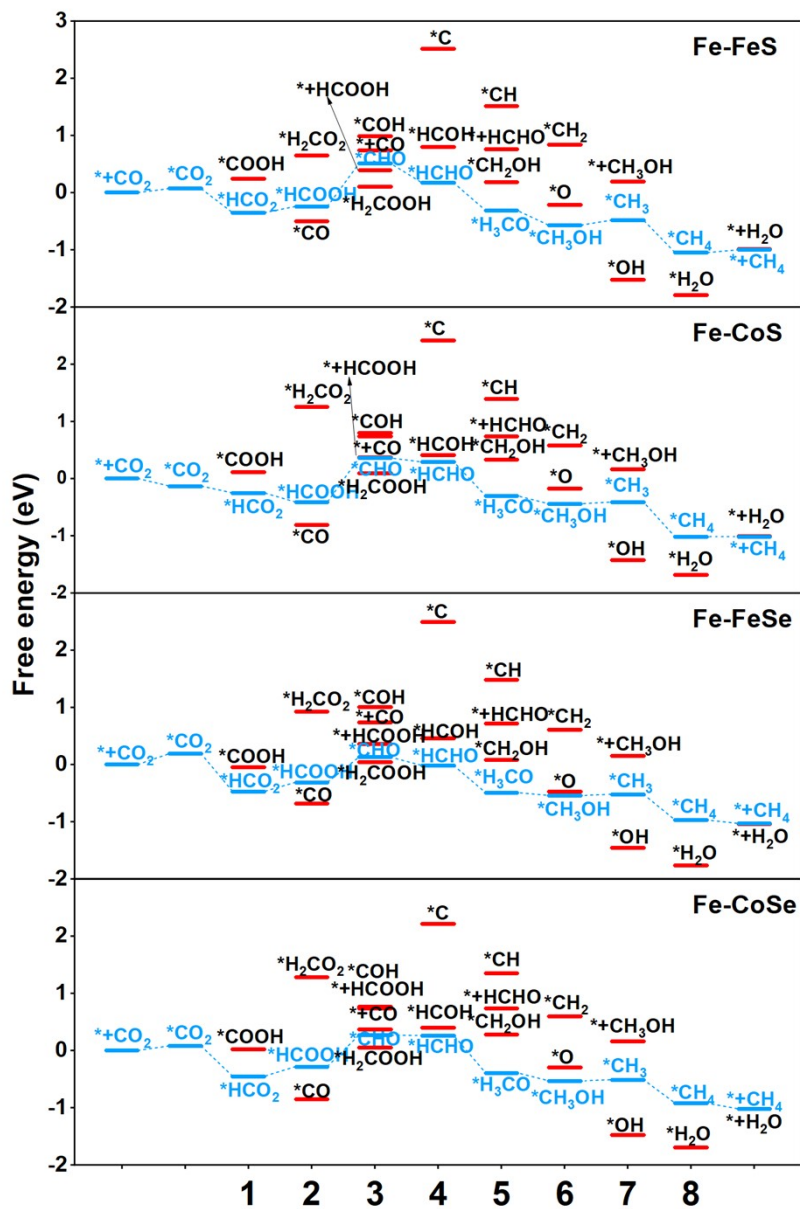
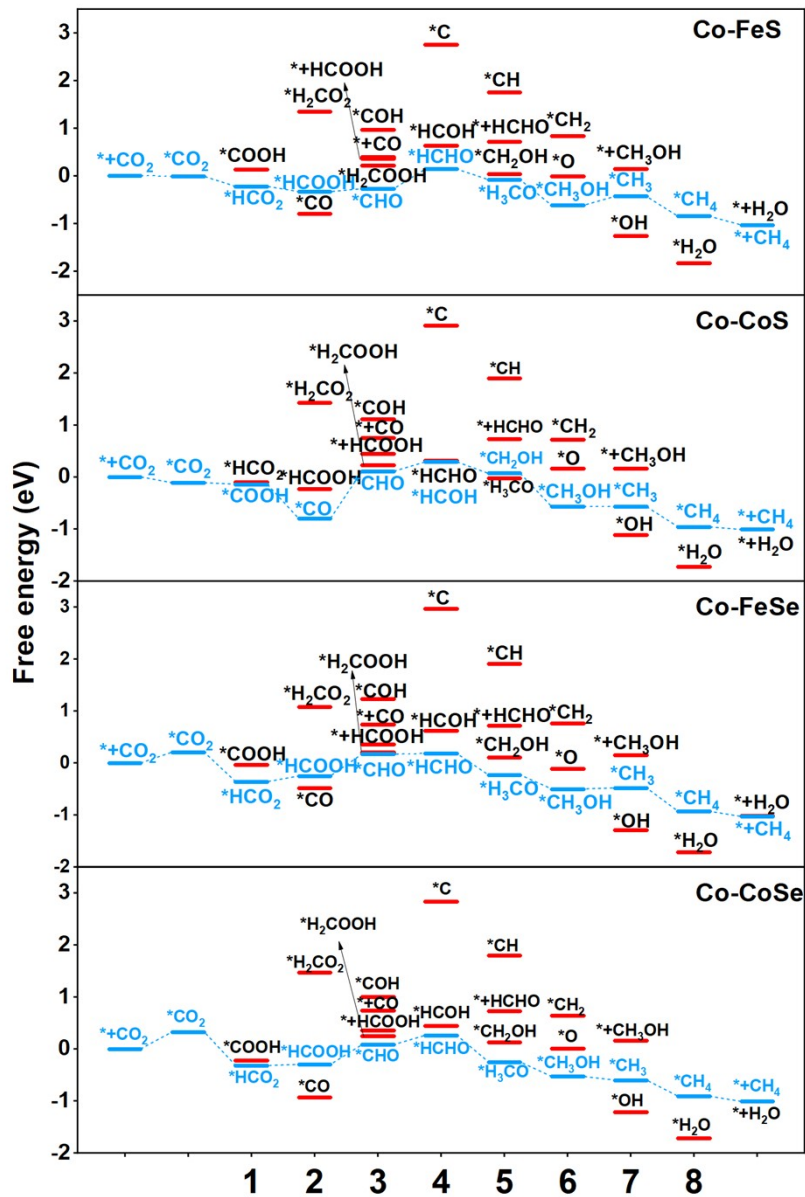


Fig. S7. The comparison between  $\Delta G_{*CO_2}$  and  $\Delta G_{*H}$ .



**Fig. S8.** Gibbs free energy diagrams of the  $CO_2$  reduction to  $CH_4$  for Fe-FeS, Fe-CoS, Fe-FeSe and Fe-CoSe.



**Fig. S9.** Gibbs free energy diagrams of the  $CO_2$  reduction to  $CH_4$  for Co-FeS, Co-CoS, Co-FeSe and Co-CoSe.

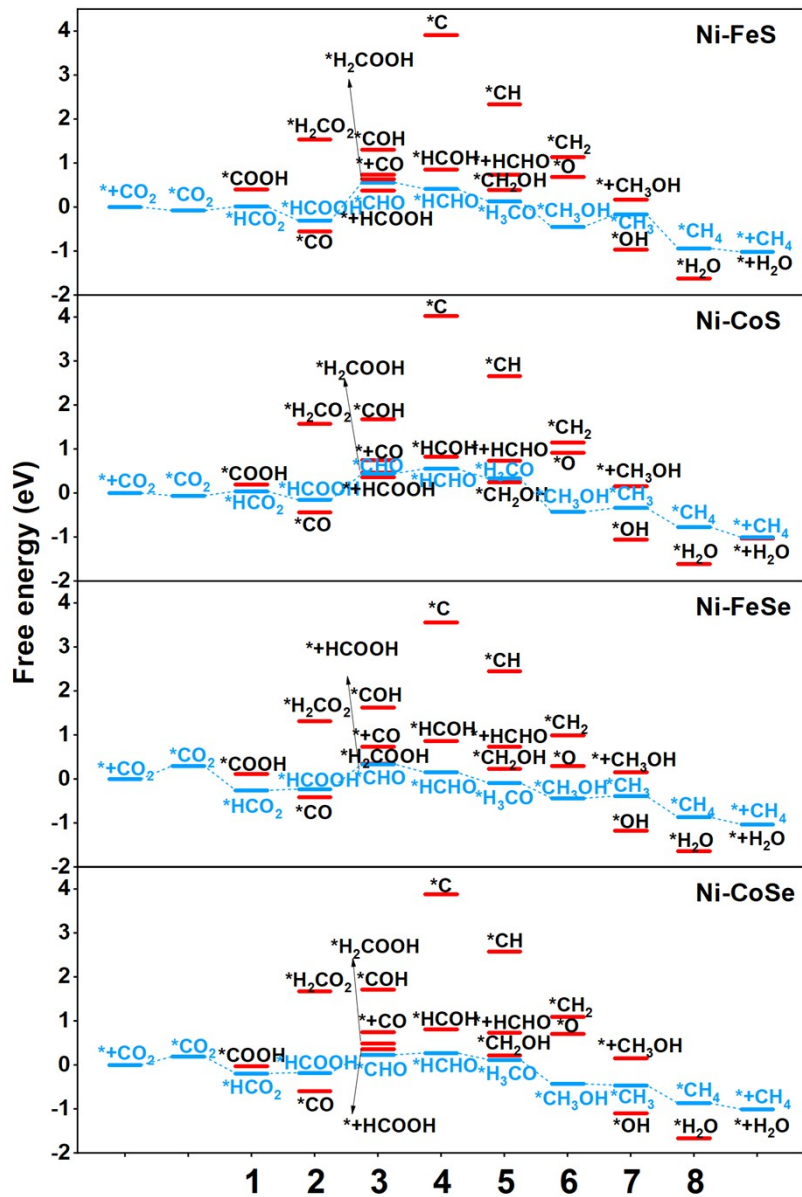


**Fig. S10.** Gibbs free energy diagrams of the  $CO_2$  reduction to  $CH_4$  for Ni-FeS, Ni-CoS, Ni-FeSe and Ni-CoSe.

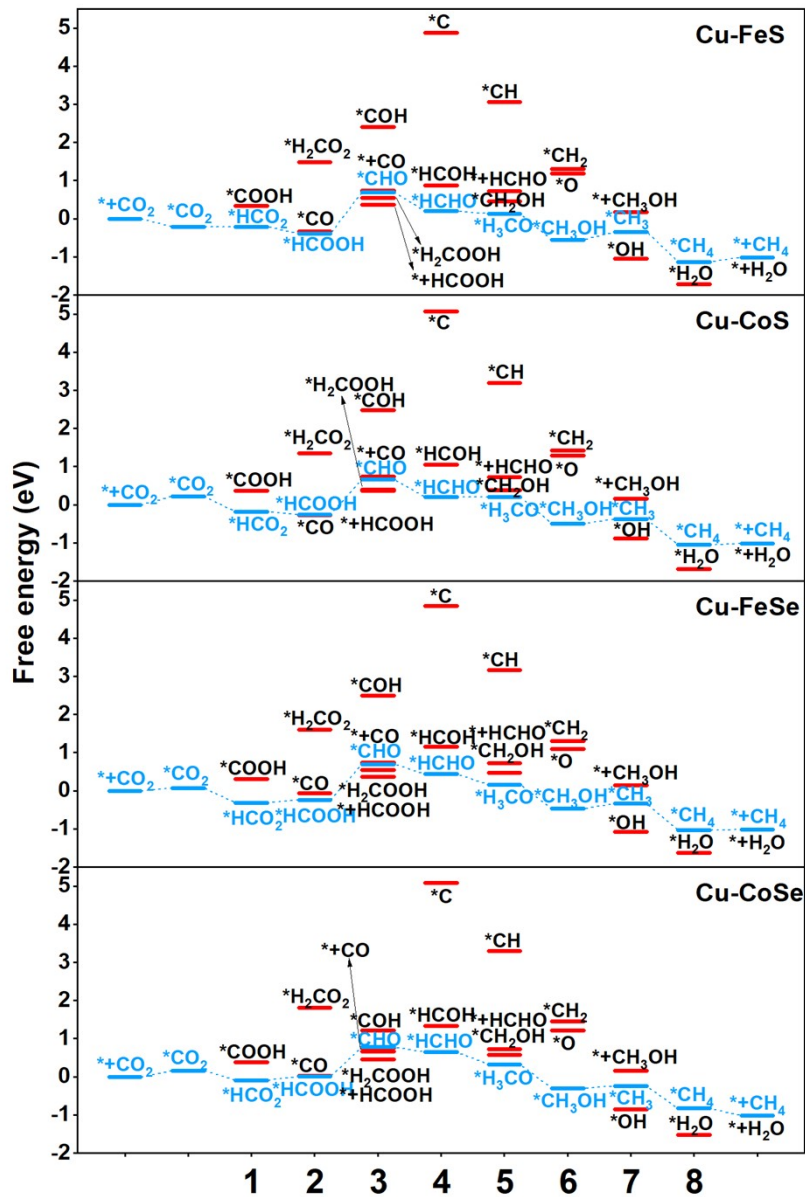


**Fig. S11.** Gibbs free energy diagrams of the CO<sub>2</sub> reduction to CH<sub>4</sub> for Cu-FeS, Cu-CoS, Cu-FeSe and Cu-CoSe.

### Fe-CoS

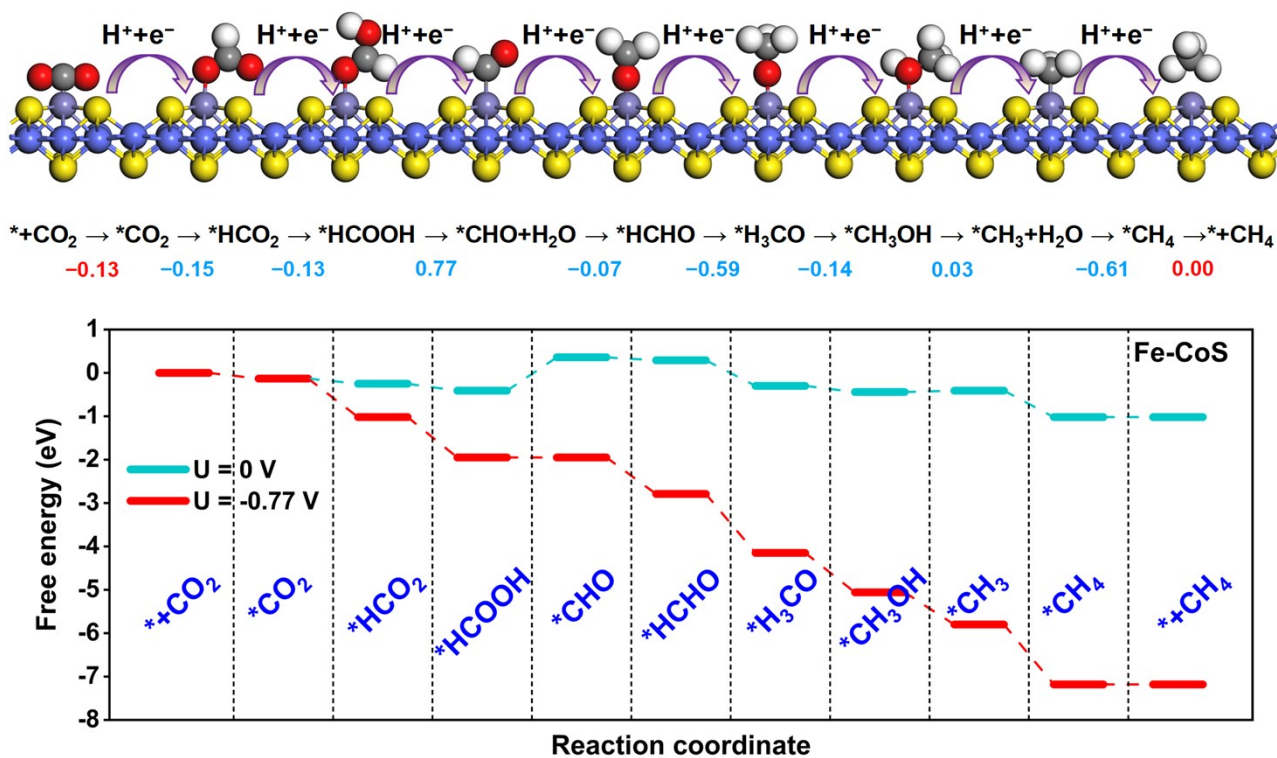
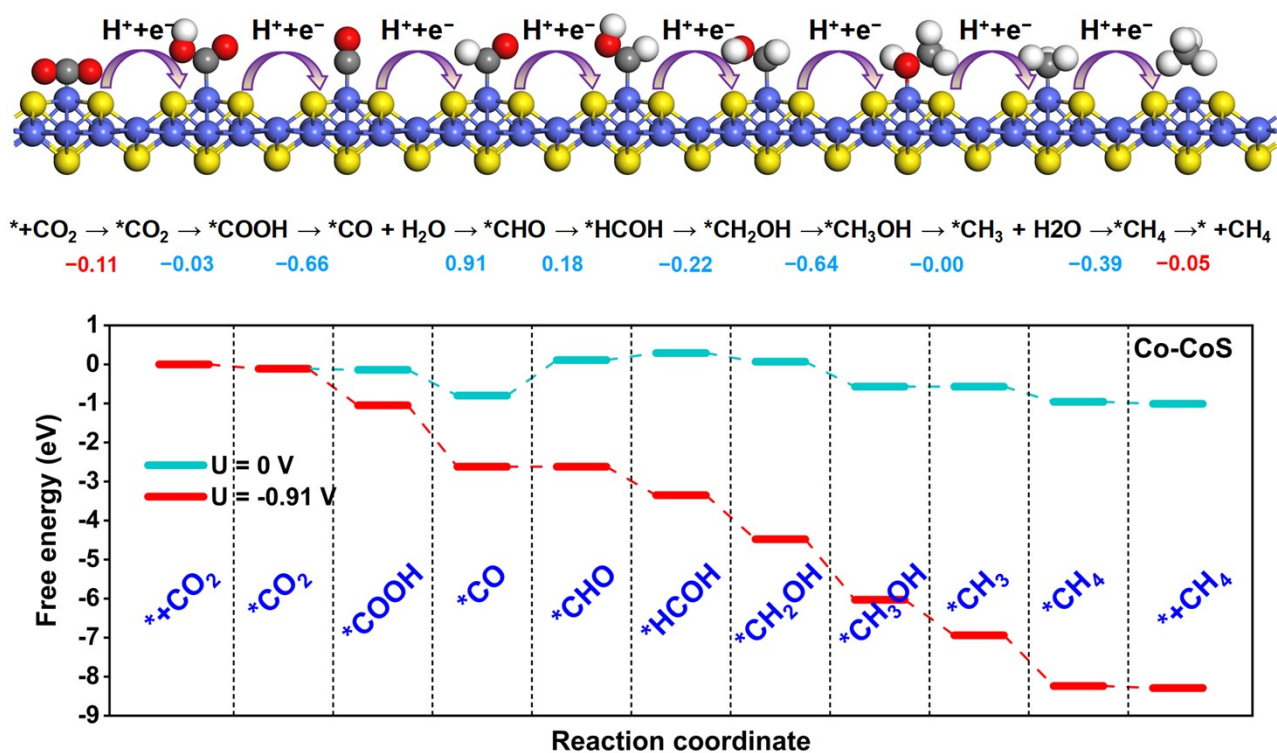
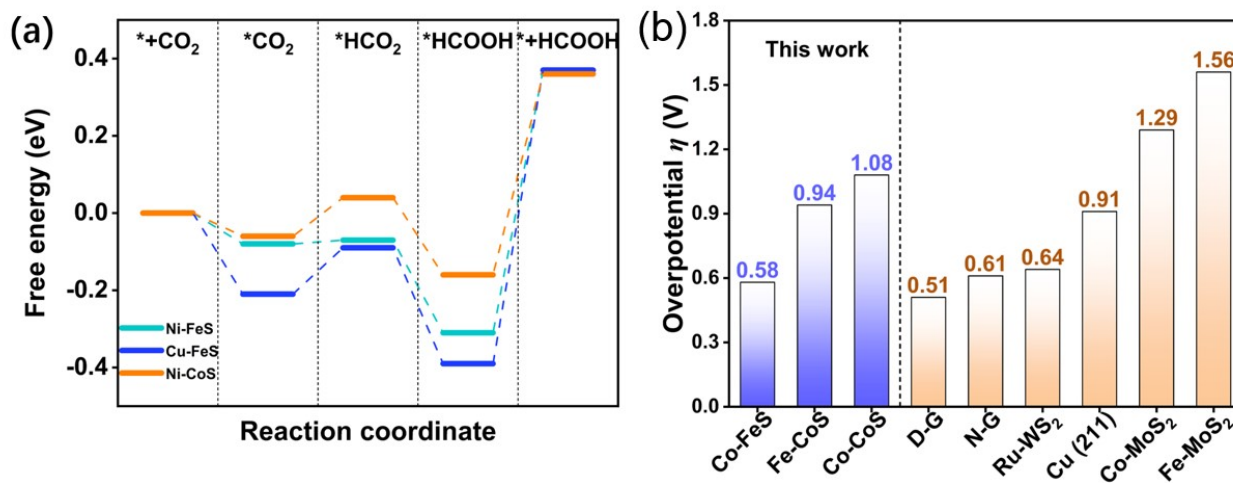


Fig. S12. Gibbs free energy diagrams of the CO<sub>2</sub> reduction to CH<sub>4</sub> for Fe-CoS along the preferred reaction pathway.

Co-CoS



**Fig. S13.** Gibbs free energy diagrams of the CO<sub>2</sub> reduction to CH<sub>4</sub> for Co-CoS along the preferred reaction pathway.



**Fig. S14.** (a) Gibbs free energy diagrams of the CO<sub>2</sub> reduction catalyzed by Ni-FeS, Cu-FeS, and Ni-CoS. (b) Overpotential comparison of our work and the reported literatures<sup>22-26</sup>.

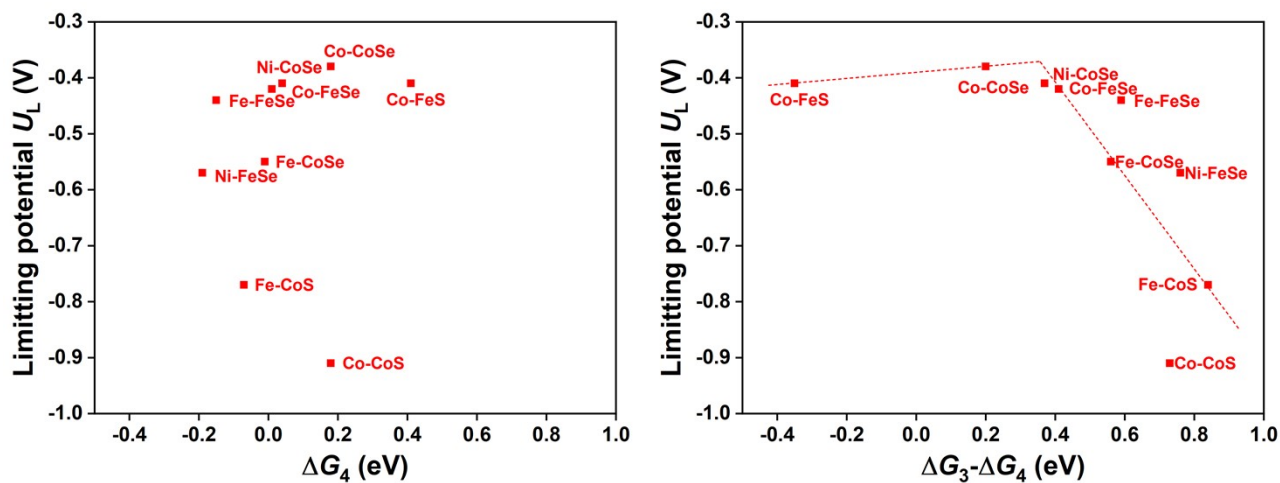


**Fig. S15.** (a) The fitting of the limiting potential  $U_L$  as a function of  $\Delta G_3$ . (b) The fitting of the limiting potential  $U_L$  as a function of  $\Delta G_3 - \Delta G_4$ .

**Table S1.** Binding energies  $E_b$ , formation energies  $E_f$ , TM Mulliken charges  $Q_{TM}$ , CO<sub>2</sub> adsorption free energies  $\Delta G^*_{CO_2}$ , CO<sub>2</sub> Mulliken charges  $Q_{CO_2}$ , length  $l_{C=O}$  of C=O bond, bond angle  $\theta_{O=C=O}$  of O=C=O, hydrogen adsorption free energies  $\Delta G^*_{H}$  ( $E_b$ ,  $\Delta G^*_{CO_2}$  and  $\Delta G^*_{H}$  in eV,  $l_{C=O}$  in Å,  $\theta_{O=C=O}$  in °,  $Q$  and  $Q_{CO_2}$  in  $e$ ).

	$E_b$	$E_f$	$Q_{TM}$	$\Delta G^*_{CO_2}$	$Q_{CO_2}$	$l_{C=O}$	$\theta_{O=C=O}$	$\Delta G^*_{H}$
Fe-FeS	-3.60	1.69	0.371	0.07	-0.150	1.250	148.460	0.27
Fe-CoS	-3.78	1.52	0.295	-0.13	0.106	1.185	179.645	0.17
Fe-FeSe	-4.64	0.65	0.232	0.19	-0.287	1.226	144.200	0.16
Fe-CoSe	-4.31	0.99	0.251	0.08	-0.248	1.259	143.318	0.10
Co-FeS	-2.95	1.79	0.140	-0.01	-0.139	1.257	145.650	0.20
Co-CoS	-3.25	1.48	0.068	-0.11	-0.153	1.260	145.085	-0.04
Co-FeSe	-4.19	0.55	0.058	0.21	-0.238	1.223	145.524	0.17
Co-CoSe	-3.48	1.25	0.024	0.33	-0.279	1.227	142.947	-0.19
Ni-FeS	-3.68	1.44	0.239	-0.08	0.091	1.185	179.169	0.46
Ni-CoS	-3.79	1.34	0.212	-0.06	0.099	1.183	179.685	0.12
Ni-FeSe	-4.59	0.54	0.158	0.30	-0.213	1.217	148.313	0.28
Ni-CoSe	-4.08	1.05	0.167	0.19	-0.269	1.221	145.888	0.05
Cu-FeS	-2.48	1.33	0.214	-0.21	0.120	1.184	179.099	0.33
Cu-CoS	-2.40	1.41	0.190	0.22	0.007	1.177	179.119	0.25
Cu-FeSe	-2.62	1.19	0.155	0.07	0.012	1.176	178.618	0.17
Cu-CoSe	-2.70	1.11	0.120	0.16	-0.001	1.176	179.543	0.34

**Table S2.** Total Gibbs free energies  $G$  of corresponding intermediate species along CO<sub>2</sub> conversion into CH<sub>4</sub> for Fe decoration.

$G$ (eV)	Fe-FeS	Fe-CoS	Fe-FeSe	Fe-CoSe
*	0	0	0	0
*CO <sub>2</sub>	0.07	-0.13	0.19	0.08
*COOH	0.24	0.11	-0.04	0.02
*CO	-0.50	-0.81	-0.68	-0.85
*COH	0.99	0.80	1.01	0.77
*C	2.51	2.42	2.49	2.22
*CH	1.51	1.39	1.48	1.35
*CH <sub>2</sub>	0.84	0.58	0.61	0.60
*CH <sub>3</sub>	-0.48	-0.41	-0.52	-0.51
*CH <sub>4</sub>	-1.05	-1.02	-0.97	-0.92
*HCO <sub>2</sub>	-0.35	-0.28	-0.47	-0.45
*H <sub>2</sub> CO <sub>2</sub>	0.65	1.25	0.93	1.28
*H <sub>2</sub> COOH	0.10	0.09	0.04	0.05
*HCHO	0.17	0.29	-0.02	0.26
*H <sub>3</sub> CO	-0.31	-0.30	-0.49	-0.39
*O	-0.21	-0.17	-0.47	-0.29
*OH	-1.52	-1.42	-1.45	-1.47
*H <sub>2</sub> O	-1.79	-1.68	-1.76	-1.69
*HCOOH	-0.24	-0.41	-0.31	-0.28
*CHO	0.51	0.36	0.13	0.27
*HCOH	0.80	0.41	0.46	0.40
*CH <sub>2</sub> OH	0.18	0.33	0.08	0.28
*CH <sub>3</sub> OH	-0.57	-0.44	-0.54	-0.53
* + CH <sub>4</sub>	-1.00	-1.02	-1.03	-1.02

**Table S3.** Total Gibbs free energies  $G$  of corresponding intermediate species along CO<sub>2</sub> conversion into CH<sub>4</sub> for Co decoration.

$G$ (eV)	Co-FeS	Co-CoS	Co-FeSe	Co-CoSe
*	0	0	0	0
*CO <sub>2</sub>	-0.01	-0.11	0.21	0.33
*COOH	0.13	-0.14	-0.03	-0.22
*CO	-0.80	-0.80	-0.48	-0.93
*COH	0.97	1.11	1.23	1.00
*C	2.75	2.91	2.97	2.84
*CH	1.75	1.90	1.91	1.80
*CH <sub>2</sub>	0.84	0.72	0.76	0.64
*CH <sub>3</sub>	-0.43	-0.57	-0.48	-0.60
*CH <sub>4</sub>	-0.85	-0.96	-0.93	-0.91
*HCO <sub>2</sub>	-0.13	-0.07	-0.36	-0.32
*H <sub>2</sub> CO <sub>2</sub>	1.35	1.43	1.08	1.47
*H <sub>2</sub> COOH	0.22	0.23	0.21	0.25
*HCHO	0.14	0.31	0.18	0.26
*H <sub>3</sub> CO	-0.08	-0.02	-0.23	-0.25
*O	-0.01	0.16	-0.11	0.01
*OH	-1.26	-1.12	-1.29	-1.21
*H <sub>2</sub> O	-1.83	-1.73	-1.71	-1.72
*HCOOH	-0.33	-0.23	-0.25	-0.30
*CHO	-0.27	0.11	0.17	0.08
*HCOH	0.63	0.29	0.62	0.44
*CH <sub>2</sub> OH	0.04	0.07	0.11	0.13
*CH <sub>3</sub> OH	-0.62	-0.57	-0.50	-0.53
* + CH <sub>4</sub>	-1.03	-1.01	-1.03	-1.01

**Table S4.** Total Gibbs free energies  $G$  of corresponding intermediate species along CO<sub>2</sub> conversion into CH<sub>4</sub> for Ni decoration.

$G$ (eV)	Ni-FeS	Ni-CoS	Ni-FeSe	Ni-CoSe
*	0	0	0	0
*CO <sub>2</sub>	-0.08	-0.06	0.30	0.19
*COOH	0.40	0.19	0.11	-0.02
*CO	-0.56	-0.44	-0.41	-0.59
*COH	1.30	1.68	1.62	1.72
*C	3.91	4.03	3.56	3.88
*CH	2.34	2.66	2.45	2.58
*CH <sub>2</sub>	1.14	1.15	0.99	1.10
*CH <sub>3</sub>	-0.17	-0.34	-0.39	-0.46
*CH <sub>4</sub>	-0.94	-0.77	-0.87	-0.87
*HCO <sub>2</sub>	-0.07	0.04	-0.26	-0.19
*H <sub>2</sub> CO <sub>2</sub>	1.54	1.57	1.31	1.68
*H <sub>2</sub> COOH	0.63	0.47	0.35	0.49
*HCHO	0.41	0.55	0.15	0.27
*H <sub>3</sub> CO	0.13	0.33	-0.09	0.12
*O	0.69	0.92	0.30	0.71
*OH	-0.97	-1.06	-1.17	-1.09
*H <sub>2</sub> O	-1.62	-1.61	-1.64	-1.66
*HCOOH	-0.31	-0.16	-0.23	-0.18
*CHO	0.56	0.44	0.34	0.23
*HCOH	0.85	0.82	0.87	0.81
*CH <sub>2</sub> OH	0.39	0.24	0.23	0.22
*CH <sub>3</sub> OH	-0.45	-0.43	-0.44	-0.43
* + CH <sub>4</sub>	-1.02	-1.01	-1.03	-1.01

**Table S5.** Total Gibbs free energies  $G$  of corresponding intermediate species along CO<sub>2</sub> conversion into CH<sub>4</sub> for Cu decoration.

$G$ (eV)	Cu-FeS	Cu-CoS	Cu-FeSe	Cu-CoSe
*	0	0	0	0
*CO <sub>2</sub>	-0.21	0.22	0.07	0.16
*COOH	0.34	0.37	0.31	0.38
*CO	-0.33	-0.27	-0.07	0.02
*COH	2.41	2.48	2.49	1.22
*C	4.88	5.07	4.85	5.08
*CH	3.06	3.19	3.17	3.30
*CH <sub>2</sub>	1.30	1.43	1.30	1.45
*CH <sub>3</sub>	-0.34	-0.38	-0.33	-0.24
*CH <sub>4</sub>	-1.13	-1.05	-1.03	-0.83
*HCO <sub>2</sub>	-0.09	-0.18	-0.31	-0.09
*H <sub>2</sub> CO <sub>2</sub>	1.48	1.35	1.60	1.81
*H <sub>2</sub> COOH	0.54	0.40	0.55	0.67
*HCHO	0.20	0.20	0.44	0.65
*H <sub>3</sub> CO	0.13	0.21	0.16	0.33
*O	1.19	1.29	1.09	1.21
*OH	-1.05	-0.88	-1.07	-0.85
*H <sub>2</sub> O	-1.72	-1.68	-1.62	-1.52
*HCOOH	-0.39	-0.26	-0.24	0.01
*CHO	0.70	0.67	0.70	0.78
*HCOH	0.88	1.05	1.15	1.34
*CH <sub>2</sub> OH	0.46	0.38	0.47	0.58
*CH <sub>3</sub> OH	-0.55	-0.49	-0.47	-0.30
* + CH <sub>4</sub>	-1.01	-1.02	-1.02	-1.02

## References

1. B. Delley, *Comp. Mater. Sci.*, 2000, **17**, 122-126.
2. B. Delley, *J. Chem. Phys.*, 1990, **92**, 508-517.
3. J. P. Perdew, K. Burke and M. Ernzerhof, *Phys. Rev. Lett.*, 1996, **77**, 3865-3868.
4. B. Delley, *Phy. Rev. B*, 2002, **66**, 155125.
5. T. Todorova and B. Delley, *Mol. Simul.*, 2008, **34**, 1013-1017.
6. L. Yang, S. H. Feng and W. H. Zhu, *J. Phys. Chem. Lett.*, 2022, **13**, 1726-1733.
7. J. Rossmeisl, Z. W. Qu, H. Zhu, G.-J. Kroes and J. K. Nørskov, *Electroanal. Chem.*, 2007, **607**, 83-89.
8. J. K. Nørskov, J. Rossmeisl, A. Logadottir, L. Lindqvist, J. R. Kitchin, T. Bligaard and H. Jónsson, *J. Phys. Chem. B*, 2004, **108**, 17886-17892.
9. A. Kulkarni, S. Siahrostami, A. Patel and J. K. Nørskov, *Chem. Rev.*, 2018, **118**, 2302-2312.
10. J. H. Montoya, C. Tsai, A. Vojvodic and J. K. Nørskov, *ChemSusChem*, 2015, **8**, 2180-2186.
11. D.-H. Lim and J. Wilcox, *J. Phys. Chem. C*, 2012, **116**, 3653-3660.
12. A. A. Peterson, F. Abild-Pedersen, F. Studt, J. Rossmeisl and J. K. Nørskov, *Energ. Environ. Sci.*, 2010, **3**, 1311-1315
13. C. N. M. Ouma, K. O. Obodo, M. Braun, G. O. Amolo and D. Bessarabov, *Appl. Surf. Sci.*, 2019, **470**, 107-113.
14. I. C. Onyia, S. O. Ezeonu, D. Bessarabov and K. O. Obodo, *Computational Materials Science*, 2021, **197**, 110613.
15. W. Zhao, L. Zhang, Q. Luo, Z. Hu, W. Zhang, S. Smith and J. Yang, *ACS Catal.*, 2019, **9**, 3419-3425.
16. Z. Li, H. Li, Z. Yang, X. Lu, S. Ji, M. Zhang, J. H. Horton, H. Ding, Q. Xu, J. Zhu and J. Yu, *Small*, 2022, **18**, 2201092.
17. G. Liu, A. W. Robertson, M. M.-J. Li, W. C. H. Kuo, M. T. Darby, M. H. Muhieddine, Y.-C. Lin, K. Suenaga, M. Stamatakis, J. H. Warner and S. C. E. Tsang, *Nat. Chem.*, 2017, **9**, 810-816.
18. Q. Wang, Z. L. Zhao, S. Dong, D. S. He, M. J. Lawrence, S. B. Han, C. Cai, S. H. Xiang, P. Rodriguez, B. Xiang, Z. G. Wang, Y. Y. Liang and M. Gu, *Nano Energy*, 2018, **53**, 458-467.
19. W. Du, Z. Sun, K. Chen, Y. Wei, R. Bao and K. Chu, *Adv. Energy Mater.*, 2024, **14**, 2401765.
20. C. Shang and Z.-P. Liu, *J. Am. Chem. Soc.*, 2011, **133**, 9938-9947.
21. Y.-w. Sun and J.-y. Liu, *Phys. Chem. Chem. Phys.*, 2023, **25**, 4773-4779.
22. Y. Linghu, T. Tong and C. Wu, *J. Phys. Chem. C*, 2023, **127**, 15035-15042.
23. A. A. Peterson, F. Abild-Pedersen, F. Studt, J. Rossmeisl and J. K. Nørskov, *Energ. Environ. Sci.*, 2010, **3**, 1311-1315.
24. M. Pu, W. Guo and Y. Guo, *ACS Appl. Mater. Interfaces*, 2023, **15**, 58388-58396.
25. S. Siahrostami, K. Jiang, M. Karamad, K. Chan, H. Wang and J. Nørskov, *ACS Sustainable Chem. Eng.*, 2017, **5**, 11080-11085.
26. H. B. Yang, S.-F. Hung, S. Liu, K. Yuan, S. Miao, L. Zhang, X. Huang, H.-Y. Wang, W. Cai, R. Chen, J. Gao, X. Yang, W. Chen, Y. Huang, H. M. Chen, C. M. Li, T. Zhang and B. Liu, *Nat. Energy*, 2018, **3**, 140-147.

